Theoretical and experimental investigation of absorption and Raman spectra of poly(paraphenylene vinylene)

E. Mulazzi and A. Ripamonti
Dipartimento di Fisica dell'Università di Milano and Istituto Nazionale di Fisica della Materia, Via Celoria 16, 20133 Milano, Italy

J. Wery, B. Dulieu, and S. Lefrant
Laboratoire de Physique Cristalline, Institut des Matériaux de Nantes, 2 rue de la Houssinière, Boîte Postale 32229, 44322 Nantes Cedex 03, France

(Received 4 June 1999)

We present experimental optical absorption and Raman data of poly(paraphenylene vinylene) (PPV) thermally converted at standard conditions at 300 °C. Theoretical calculations of the band shapes of both optical absorption and Raman spectra of standard PPV are reported, based on spectroscopic properties of known polymeric chains of different lengths. In particular, we have focused our study on the dependence of the Raman band intensities on the excitation wavelengths, taking into account the intensity changes observed in the Raman spectra of the oligomers. Such calculations are carried out by considering the electronic energies of optical transitions, the most intense Raman active vibrational frequencies, and the interactions between these vibrations and the electronic states of the oligomers considered. We show that the experimental data of optical absorption and Raman spectra can be theoretically accounted for, if a distribution of conjugated segments of different lengths is introduced in the evaluations. [S0163-1829(99)01948-7]

I. INTRODUCTION

Poly(paraphenylene vinylene) (hereafter referred to as PPV) is still nowadays extensively studied due to its ability to be used in light emitting diodes or devices made with polymeric compounds.[1,2] In this respect synthesis conditions are of prior importance for the electronic properties of such materials in terms of reliability and reproducibility. As a matter of fact, the precursor route for making conjugated materials such as PPV allows one to modify the synthesis parameters with the purpose of preparing polymers with specific properties. So-called standard PPV is achieved by thermal treatment at 300 °C under dynamic vacuum, whereas photopolymerized PPV is obtained at lower temperature and exhibits slightly different properties, as shown by spectroscopic data.[3,4] In addition, doping conditions in this latter case turn out to the different with respect to those of standard PPV, due to an increase of $|\vec{a}|$ and $|\vec{b}|$ parameters of the monoclinic unit cell and also to different average conjugation length of the segments, in the polymeric compound.[3]

In this paper, we restrict our study to standard PPV and present both experimental and theoretical results obtained for this polymer in optical absorption and Raman scattering spectra. All measurements have been carried out at room temperature. Raman spectra have been recorded at different excitation wavelengths chosen in the appropriate spectroscopic range, in order to avoid a strong fluorescence signal. Therefore we have used wavelengths in the near infrared $\lambda_L = 1064$ nm, in the red range at $\lambda_L = 676.4$ nm, and also in the near UV at $\lambda_L = 363$, 351.1, and 333.3 nm.

The band shapes in both optical-absorption and Raman scattering spectra have been calculated by using the same electron-vibration interactions which are responsible of the vibronic structure and of the band intensities in the two optical spectroscopic linear responses, respectively. These evaluations were achieved by considering the vibronic structures observed in the absorption spectra of oligomers[5] of different lengths and reproducing the main features of Raman spectra of the same compounds.[6,7] The more important characteristics of the absorption and Raman bands of standard PPV are then calculated by weighting the contributions through a distribution of conjugated PPV segments of different lengths, as was been reported previously in order to explain the spectroscopic features in other conducting polymers.[7,8] In the present case, we have chosen a bimodal Gaussian distribution in order to weight the different contributions to the absorption and Raman band shapes in an asymmetric way.

II. EXPERIMENTAL RESULTS

In Fig. 1 we present, for purposes of comparison, the absorption curves recorded at room temperature of PPV

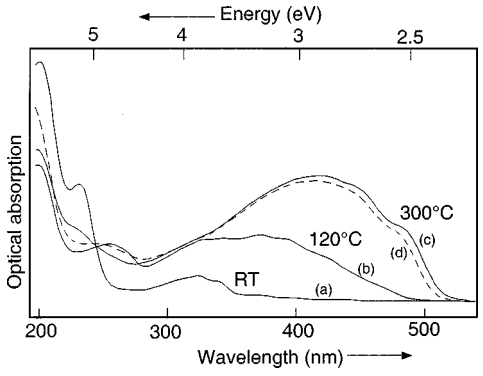

FIG. 1. Optical-absorption spectra, recorded at room temperature, of the precursor polymer converted at different temperatures: (a) 20 °C. (b) 120 °C. (c) 300 °C. (d) Photoconverted sample at 120 °C under UV illumination for 30 min.

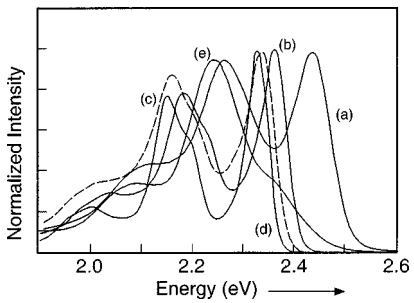

FIG. 2. Photoluminescence spectra recorded at 10 K of PPV: (a) thermally converted at 120 °C; (b) thermally converted at 300 °C; (c) photoconverted at 120 °C; (d) the same sample of (b) at 80 K; (e) the same sample of (b) at 300 K.

samples obtained in different conditions together with the optical-absorption spectrum of a sulphonium salt precursor polymer at room temperature. PPV thin films are prepared by thermal conversion in vacuum at different temperatures [Figs. 1(b) and 1(c)] or by photoconversion at 120 °C [Fig. 1(d)]. Then we focus on the optical properties of so-called standard PPV, i.e., prepared under termal treatment at 300 °C. Let us note that the absorption features of the PPV sample photopolymerized under optimized conditions are close to those of standard PPV [Figs. 1(c) and 1(d)]. This result is corroborated by photoluminescence (PL) measurements carried out at 10 K (Fig. 2), in which the various bands, observed for both standard PPV and the photoconverted sample, are also close to each other [see Figs. 2(b) and 2(c)]. In the same figure, curves (d) and (e), we show also the effect of temperature on PL spectra of standard PPV (termally converted at 300 °C). As can be seen, the increase of temperature modifies the PL features, as observed previously by Yu *et al.* (Ref. 9). In this reference this effect was explained in terms of disorder induced by the increase of temperature, affecting the distributions of conjugation lengths. The same effect is also observed in the UD visible absorption spectrum, as we report in Fig. 3.

In Figs. 4(a)–4(d), we show the absorption curves of the different oligomers of PPV from 2–5 phenyl rings, (which according to the notation of Ref. 5 we call PPV2 (TSB, transtilbene), PPV3 (DSB, distiryl benzene), PPV4 (DSV, distiryl vinyl vinylene), and PPV5 respectively. These spectra recorded at 80 K, taken from Ref. 5, are presented together with the optical absorption spectrum of standard PPV

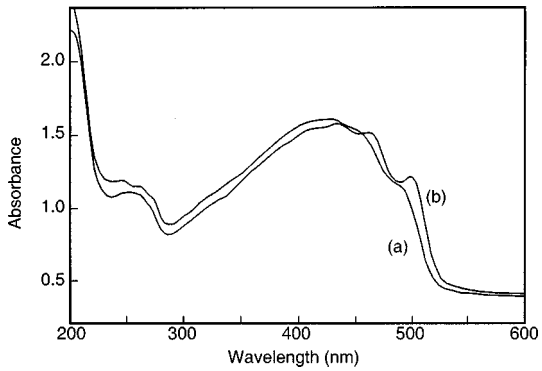

FIG. 3. Absorption spectrum of standard PPV recorded at (a) 300 and (b) 78 K.

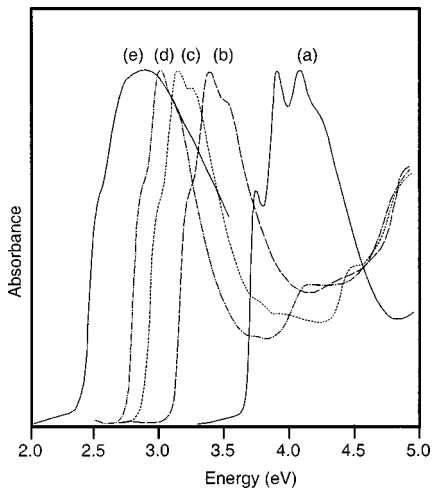

FIG. 4. Experimental absorption spectra of PPV and PPV oligomers: (a), (b) (c) and (d) are the absorption curves of PPV2, PPV3, PPV4, and PPV5, respectively, taken from Fig. 2 of Ref. 5 and recorded at $T=80$ K. (e) Absorption curve of standard PPV recorded at 300 K.

recorded at room temperature. By this figure we show that the features of the absorption band of PPV can be regarded as a superposition of the different contributions of the optical absorptions of the oligomers in the range 2.5–5 eV.

In Fig. 5 we show the Raman spectra of standard PPV recorded at room temperature for different excitations wavelengths λ_L from near IR to near UV. The frequencies of the maximum of the most intense Raman bands, which are due to the stretching vibration of the vinyl group and of the phenyl ring, do not depend significantly on the laser excitation wavelengths, and they are located at 1174, 1330, 1550, 1586, and 1628 cm^{-1}, respectively. A complete analysis of the vibrational modes in PPV has been given in Ref. 6, and in Table I we just recall the main assignment of the five modes we consider in this paper, and in particular in the theoretical calculations. Conversely, from the spectra shown in Figs. 5(a)–5(c), the most striking result comes from the relative intensity of the bands, which changes noticeably with the laser light. In particular, as it can be observed from these

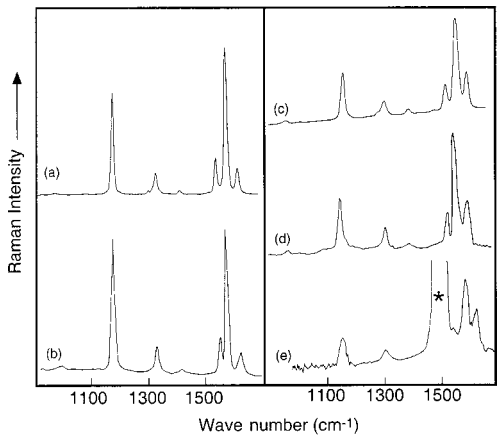

FIG. 5. Experimental Raman spectra of standard PPV recorded at 300 K for different excitation wavelengths: (a) 1064, (b) 676.4, (c) 363.8, (d) 351.1, and (e) 333.3 nm. The asterisk indicates the presence of a strong plasma line issued from the argon laser.

TABLE I. Assignment of the most intense Raman active vibrational modes of (PPV). The values of the vibrational frequencies given here are used in Eqs. (1), (2), (4) and (5).

f	Frequency ω_f	Main assignment
1	1174 cm^{-1}	C—C stretching +C-H bending of the phenyl ring
2	1330 cm^{-1}	C═C stretching +C-H bending of the vinyl group
3	1550 cm^{-1}	C═C stretching of the phenyl ring
4	1586 cm^{-1}	C—C stretching of the phenyl ring
5	1625 cm^{-1}	C═C stretching of the vinyl group

figures, the ratios of the intensity of the band peaked at 1174 cm^{-1} (I_{1174}) with respect to that of the band peaked at 1586 cm^{-1} (I_{1586}) and to the one at 1628 cm^{-1} (I_{1628}) exhibit an increase when the laser light is tuned from $\lambda_L = 1064$ nm to $\lambda_L = 676.4$ nm, [Figs. 5(a) and 5(b), respectively]. Conversely, these ratios decrease drastically by using a laser light λ_L in the near-UV wavelength region [see Figs. 5(c), 5(d), and 5(e)]. Furthermore, the intensity ratio I_{1550}/I_{1628} has a peculiar behavior with respect to the other two, reported above. In fact, this ratio is larger than one in the spectra recorded with λ_L in the near-IR frequency region, while it becomes less than one in the spectra observed with λ_L in the near-UV region. This behavior can be related to the changes observed in the relative intensity of the Raman bands of oligomers. To illustrate this, in Figs. 6(a)–6(c) we show their Raman spectra recorded at room temperature for $\lambda_L = 1064$ nm. We have chosen this excitation wavelength in order to avoid resonance effects, and to be able to compare band intensities of these different oligomers, with respect to the one of standard PPV [Fig. 6(d)]. These oligomers are, according to the notation introduce above, PPV2 (TSB, transtilbene), PPV3 (DSB, distyrilbenzene), and PPV4 (DSV, distiryl vinyl vinylene). From these figures, we may observe changes in the ratio I_{1174}/I_{1628}, which increases with the number of phenyl rings, and in the ratio I_{1628}/I_{1586}, which decreases with this number. This behavior, very clearly observed also in Figs. 6, is a consequence of the nature of the vibrational modes involved in Raman scattering of these oligomers.

III. THEORETICAL RESULTS

We have calculated the shapes of the bands observed in the optical-absorption spectra of standard PPV and its related oligomers. In addition we have evaluated the relative intensities and the shapes of the bands due to the stretching vibrations listed in Table I, observed in Raman-scattering (in preresonance and resonance conditions) spectra of the same polymeric compounds. These calculations have been performed by using a model in which both the optical response functions are evaluated in terms of the same formalism. In this way, the shapes and the relative intensities of the Raman bands considered are calculated by using the same values (for example, the electron-vibration interaction couplings and the distribution of the conjugated segments) found in the calculations of the optical, absorption band shapes. In fact, the interactions between the electron in the excited state and the stretching vibrations, which are responsible for the optical-absorption band shapes, are also responsible for the intensities of the bands observed in the Raman spectra.

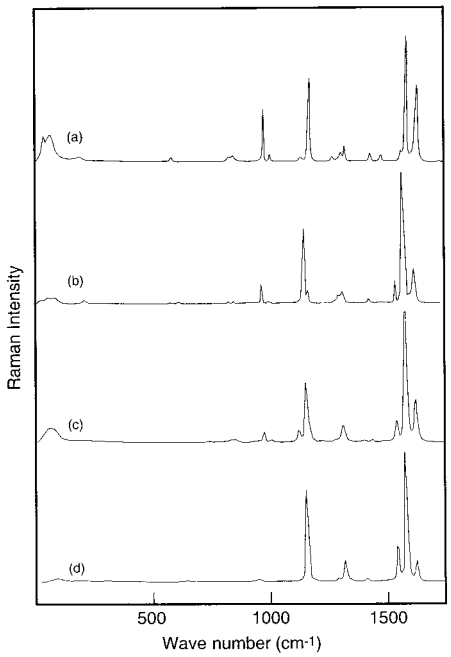

FIG. 6. Experimental Raman spectra of PPV oligomers and of a standard PPV sample recorded at room temperature for $\lambda_L = 1064$ nm: (a) TSB (transtibene), (b) DSB (distyrilbezene), (c) DSV (distyril-vinylvinilene), and (d) PPV.

The major purpose of these calculations is to show that the absorption and Raman, scattering band shapes of standard PPV are well interpreted in terms of the contribution of the different oligomers weighted by a distribution of conjugated segments. Moreover, the change of the relative intensities of the Raman bands as a function of the laser wavelengths, as experimentally observed, can be interpreted in a straightforward way on the basis of this model.

In the following, we give the function we have used in the evaluation of the optical-absorption band shape[7] and intensity for the different oligomers whose number of repeating units (phenyl rings) are indicated by n (for the oligomers considered here $n = 2-10$)

$$I(\Omega,n) = |M_n|^2 \left\{ \sum_{j=0}^{2} \sum_{f=1}^{5} \exp\left[-\sum_{f=1}^{5} S_{f,n} \right] \frac{(S_{f,n})^j}{j!} \times \frac{\gamma_n}{(\Omega - \Omega_n - j\omega_j)^2 + \gamma_n^2} \right\}. \quad (1)$$

M_n is the electric dipole moment intensity for the electric transition to the $1B_u$ state of each oligomer with n phenyl rings,[10] whose frequency is indicated by Ω_n. $j = 0$, 1, and 2 numbers the vibronic processes considered in the following calculations (up to two vibronic processes). $S_{f,n}$ are the contributions to the total Huang-Rhys factors $S_n = \Sigma_{f=1}^{5} S_{f,n}$, which come from each vibrational mode (labeled by f) interacting with the electronic excited state $1B_u$ of every oligomer with n phenyl rings. These contributions are related to the electron-vibrational couplings for each vibrational stretching mode we consider here ($f = 1-5$), and whose frequency is indicated by ω_f. The values of the stretching mode frequencies ω_f are given in Table I together also with

TABLE II. Values of Ω_n, $S_{f,n}$, S_n, and γ_n (at $T=78$ and 300 K) used in Eqs. (1), (2), (4), and (5) for the calculations of absorption and Raman band shapes of different PPV samples.

n	2	3	4	5	6	7–10
Ω_n (eV)	4.48	3.88	3.53	3.47	2.85	2.60
$S_{1,n}$	0.40	0.40	0.42	0.45	0.50	0.52
$S_{2,n}$	0.10	0.08	0.08	0.08	0.08	0.08
$S_{3,n}$	0.12	0.12	0.12	0.15	0.20	0.20
$S_{4,n}$	0.96	0.95	0.92	0.92	0.75	0.70
$S_{5,n}$	0.32	0.25	0.23	0.15	0.15	0.10
S_n	1.90	1.80	1.77	1.75	1.70	1.60
γ_n (eV) $T=78$ K	0.09	0.10	0.10	0.10	0.11	0.11
γ_n (eV) $T=300$ K	0.12	0.12	0.14	0.16	0.18	0.20

the relative assignment. In this paper, we do not take into account any change of ω_f with the length of the segments. The values of M_n are taken from Ref. 10. In Table II, we give Ω_n, $S_{f,n}$, S_n, and the damping factors γ_{n-} for $T=78$ and 300 K. Ω_n have been evaluated in the same approximation as in Ref. 5, and they are in agreement with the data reported there. $S_{f,n}$ are fitted from the Raman experimental spectra of the oligomers, taking into account also the properties of the electron vibrational couplings in the $1B_u$ excited states for intermediate and short segments.[7] As it can be seen from Table II, $S_{f,n}$ change as a function of the stretching mode frequencies $\omega_f(f=1-5)$ and of the number of the phenyl rings, n. In particular $S_{1,n}$ and $S_{3,n}$ increase for n going from 2 to 10, while $S_{4,n}$ and $S_{5,n}$ decrease and $S_{2,n}$ do not show a significant change in the same range of n. This is due to the different behaviors of the five-electron vibrational couplings coming from the decreasing localization of the electronics states $1B_u$ for increasing n. It is worth stressing that while $S_{f,n}$ have different behaviors as a function of increasing n, the values of S_n decrease in the same range of n (see Table II) from 1.90 for $n=2$ to 1.60 for $n=7-10$. This trend is consistent with the result that overall electron vibrational interaction couplings always increase as function of the localization of the electronic states, as it found in many oligomers.[5]

In Fig. 7, we show the calculated absorption band shapes for the different oligomers with $n=2$, 3, 4, and 6 at 78 K. One can see that there is a very good agreement between the experimental data of Ref. 5 and the band shapes given in Fig. 7. Let us point out that the vibronic structures in the band shapes of Fig. 7 are more evident in the absorption of short oligomers, since the overall interactions between the stretching vibrations and the electronic states are always more intense in localized states.

In order to calculate the optical absorption band shape $I(\Omega)$ of PPV, we use the expression

$$I(\Omega)=\sum_{n=2}^{10} I(\Omega_n)\times P_n. \tag{2}$$

In Eq. (2), we have weighted the contributions $I(\Omega_n)$ of the single oligomer with n phenyl rings with P_n, the double Gaussian distribution given in Eq. (3),

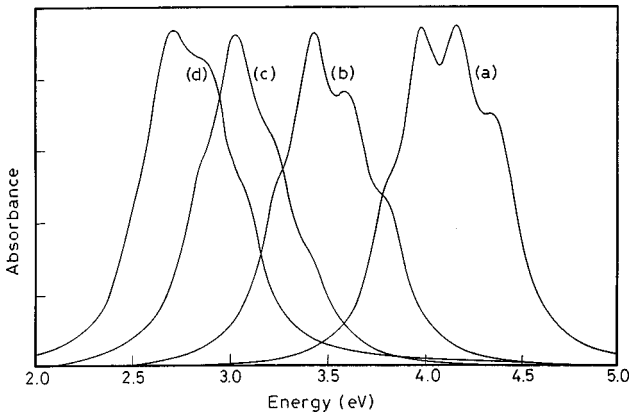

FIG. 7. Calculated absorption curves of different PPV oligomers at $T=80$ K, using Eq. (1) and the values of parameters of Table II: (a) PPV2, (b) PPV3, (c) PPV4, and (d) PPV6.

$$P_n=\frac{1-G}{(2\pi\sigma_1)^{1/2}}\exp-\left(\frac{n-n_1}{2\sigma_1}\right)^2+\frac{G}{(2\pi\sigma_2)^{1/2}}\times\exp-\left(\frac{n-n_2}{2\sigma_2}\right)^2, \tag{3}$$

where n_1 and σ_1 are the values of the most probable segment lengths and the related dispersion, respectively, of the distribution for $n=2-6$ (short oligomers), while n_2 and σ_2 are the values for the parameters related to the distribution for $n=7-10$ (intermediate length oligomers). G is the weight of the second distribution with respect to the first one.

In Figs. 8(a) and 8(b) we give the absorption band shapes calculated for two different sets of distribution parameters given in Table III and by using the values of ω_f, Ω_n, $S_{f,n}$, S_n, and γ_n given in Tables I and II. These figures are in very good agreement with the experimental data: Fig. 8(a) with the absorption band of standard PPV recorded at room temperature given in Fig. 3(a), and Fig. 8(b) with the absorption band shape of an ''improved'' PPV sample at room temperature, given in Fig. 2 of Ref. 11. Notice that for the band shapes given in Figs. 8(a) and 8(b), the value of n_2 is always centered on 7, while G is different for Fig. 8(a) with respect to Fig. 8(b). This indicates that for this last band shape, characterized by a higher value of G, the more important contri-

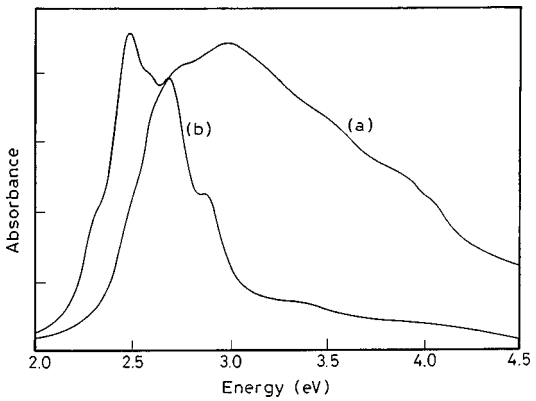

FIG. 8. Calculated absorption curves at $T=300$ K. using Eqs. (2) and (3) and the values of parameters of Tables II and III: (a) standard PPV sample; (b) ''improved'' PPV sample.

TABLE III. Distribution parameters used in the calculations of Raman and absorption band shapes [Eqs. (2)–(5)] for different PPV samples at $T=78$ and 300 K.

	n_1	σ_1	n_2	σ_2	G
Fig. 8(a)	3	1	7	2	0.3
Fig. 8(b)	4	1	7	2	0.95
Fig. 9	4	1	8	2	0.4

butions come only from intermediate segments. Conversely, the absorption band shape of standard PPV given in Fig. 8(a) is determined by a distribution where intermediate ($n=7-10$), and short ($n=2-6$) oligomers bring comparable contributions.

In Fig. 9 we give the absorption band shape at 78 K which simulates the experimental absorption data given in Fig. 3(b). The parameters of the distribution used in these evaluations are given in Table III, while the values of the ω_f, Ω_n, S_n and γ_n at different temperatures, are given in Tables I and II. The parameters used for Fig. 9 indicate that by lowering the temperature the effective length of the segments becomes in ''average'' longer with respect to the case of standard PPV at room temperature, since the disorder decreases with the temperature, influencing in this way the values of n_2 and G in the distribution we use in the simulation. Furthermore, the structures in the band shape are more defined with respect to the case of Fig. 8(a), since a lower disorder determines, as a consequence, a slight decrease of γ_n.

In order to calculate the Raman scattering in resonance or in preresonance (RRS) conditions for PPV, we use the functions $\alpha_f(\Omega_L,\omega)$ the first order RRS cross sections for each vibrational frequency ω_f considered, given in the equation.

$$\alpha_f(\Omega_L,\omega)\approx\sum_{n=2}^{10}|M_n|^4 S_{f,n}\times\left|\sum_{l=0}^{1}(-)^l R_n(\Omega_L-l\omega_f)\right|^2 \times\frac{1}{\sqrt{2\pi\Delta_f}}\exp-\left(\frac{\omega-\omega_f}{2\Delta_f}\right)^2\times P_n \tag{4}$$

where Ω_L is the laser excitation frequency, ω is the frequency in the Stock range, Δ_f is the width of the Raman band considered whose maximum is at ω_f, and P_n is the distribution given in Eq. (3). The functions $R_n(\Omega_L-l\omega_f)$ for $l=0$ and 1, which weight the cross section for each oligomer of length n, are given by the equation.

$$R_n(\Omega_L)=\exp\left[-\sum_{f=1}^{5}S_{f,n}\right]\sum_{j=0}^{2}\sum_{f=1}^{5}\frac{(S_{f,n})^j}{(j)!}\times\frac{\gamma_n+i(\Omega_L-\Omega_n-j\omega_f)}{\gamma_n^2+(\Omega_L-\Omega_n-j\omega_f)^2} \tag{5}$$

In Figs. 10(a)–10(d), we give the calculated RRS spectra of standard PPV at room temperature, by using Eqs. (4) and (5) and the parameters given in Tables I–III. In these calculations we have not considered any change of ω_f as a function of n nor Δ_f as a function of f, and have taken $\Delta_f=\Delta=7\ \mathrm{cm}^{-1}$. The band shapes and intensities in the RRS spectra shown in Figs. 10(a)–10(d) are calculated for $\lambda_L=676.4$, 363.8, 351.1, and 333 nm, respectively. From these figures, we note that the change of the ratio of I_{1550}/I_{1628} is in very good agreement with what has been experimentally observed. In fact from being larger than one for Ω_L in the red frequency region, it becomes less than one for Ω_L in the UV region. This behavior is determined by the change of coupling interactions between the electronic states of the oligomers of different conjugation length and the vibrations at 1550 (stretching of phenyl ring) and 1628 cm^{-1} (double bond stretching of the vinyl group). In fact in intermediate conjugated segments, the electronic states have a relatively stronger interaction with the mode at 1550 cm^{-1}, compared to the one at 1628 cm^{-1}. Conversely, in short conjugated segments the stronger interaction occurs between the elec-

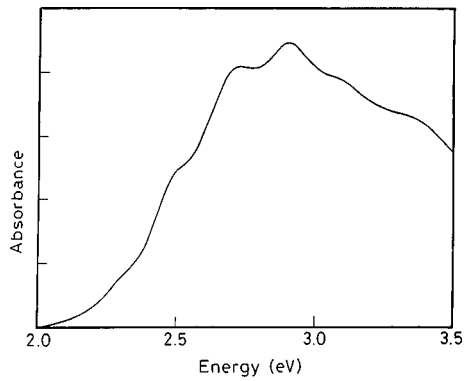

FIG. 9. Calculated absorption curve of standard PPV [by using Eqs. (2) and (3)] at $T=78$ K. Parameters are given in Tables II and III.

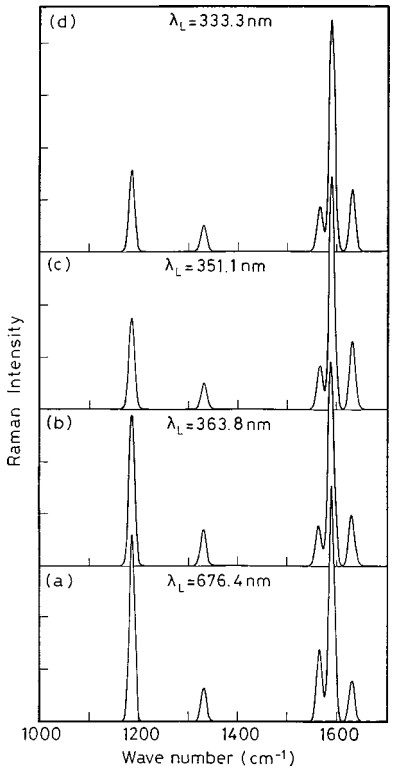

FIG. 10. Calculated Raman band shapes of the five most intense vibrational modes considered for standard PPV, by using Eqs. (4) and (5) and the values of parameters of Tables II and III: (a) $\lambda_L=676.4$ nm, (b) $\lambda_L=363.8$ nm, (c) $\lambda_L=351.1$ nm, and (d) $\lambda_L=333.3$ nm.

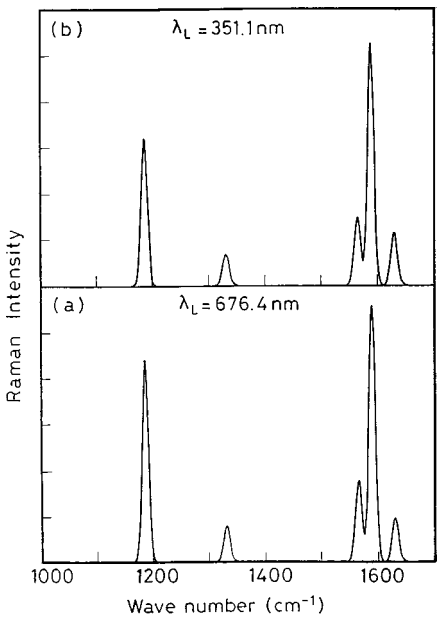

FIG. 11. Calculated Raman band shapes of ''improved'' PPV for the same modes as in Fig. 10 and for $\lambda_L = 676.4$ nm (a) and 351.1 nm (b). The parameters are given in Tables II and III.

tronic states and the mode at 1628 cm^{-1}, due to the high localization of these electronic states. Since short and intermediate conjugated segments contribute to the distribution which simulates the standard PPV in a comparable way (see Table III), the observed change in the ratio is only determined by the resonance conditions of Ω_L.

From Fig. 10, we can see that the ratios of I_{1174}/I_{1586} and I_{1174}/I_{1628} also decrease when the laser light is tuned from the red to the UV frequency region. These results again are explained in terms of the changes of the electron vibrational couplings related to these frequencies, from the values in intermediate segments to those in short segments. In fact the interaction of the electronic states and the single bond stretching mode at 1174 cm^{-1} becomes stronger in intermediate conjugated segments, while the interactions with the modes at 1586 and 1628 cm^{-1} are relatively stronger in short conjugated segments. Then, as before, the changes in the ratio in the calculated spectra, in agreement with those observed in the experimental spectra, are explained in terms of the resonance conditions of Ω_L with the electronic transitions of intermediate and short conjugated segments.

In order to corroborate our results, in Fig. 11 we show the calculated Raman band shapes for the ''improved'' PPV, whose experimental absorption is shown in Fig. 2 of Ref. 11, and for which the calculated absorption curve is given in Fig. 8(b). For the calculation of the Raman band shapes of Fig. 11, we have used the same values of Ω_n, $S_{f,n}$, S_n, and γ_n of Table II, and the parameters of Table III, already chosen and utilized in the calculation of the absorption curve given in Fig. 8(b). As can be observed from Fig. 11, the changes of the ratios discussed above, i.e., I_{1550}/I_{1628}, I_{1174}/I_{1586}, and I_{1174}/I_{1628}, are not significantly dependent on the excitation wavelengths, indicating that only intermediate length segments predominate in the sample and that the contributions of short oligomers are negligible.

IV. DISCUSSION AND CONCLUSION

In this paper, we have shown the results of the simulation of the absorption spectra of standard PPV converted at 300 °C, at 78 K, and 300 K, and of the ''improved'' PPV at 300 K. In a parallel way, by using the same parameters listed in Tables II and III, we have calculated the band shapes and relative intensities of the five most intense vibrational modes of standard PPV, and of the ''improved'' PPV, at different excitation wavelengths at 300 K. The calculations were performed by taking into account the electronic states, the vibrational modes, and the interactions of the oligomers.

Good agreement is found between calculated and experimental spectra, by considering a double distribution of conjugation lengths, whose two maximum peaks are in the range $n = 2-6$ and 7–10, respectively. In general, the overall distributions we have used (Table III) are asymmetric, as already reported in Ref. 12 for polyacetylene segments in diblock copolymers, where distributions of conjugated segments similar to those considered in this paper have been introduced. Let recall that the same parameters are used in the evaluations of the absorption and Raman spectra, providing a coherent model for the polymeric sample in terms of conjugation lengths.[7,12]

In particular we have introduced in both the calculations the electron vibrational couplings $S_{f,n}$ (see Table II), which change as a function of the stretching mode frequencies ω_f and of the electronic state of different oligomers with n phenyl rings. Moreover, the sum of these parameters leads to the total Huang-Rhys factors, which show a decreasing trend as function of n, as discussed previously. We want to stress that this evolution of S_n as a function of n is also consistent with the progressive softening of the relaxation processes occurring upon photoexitation of electron-hole pairs in different oligomers with n phenyl rings.[5]

The introduction of $S_{f,n}$ together with the other parameters of Tables II and III in the calculation has in particular allowed an evaluation of the change of the calculated intensity ratios between specific. Raman bands, as a function of excitation wavelengths, in very good agreement with the experimental data (see Figs. 5 and 10). As a consequence, Raman scattering comes out as a nondestructive and powerful technique which allows one determine an average effective length in the polymeric film. As a matter of fact, there is a close relationship between x-ray data and the results obtained from the Raman spectra and their interpretations in terms of crystallinity (see Figs. 4 and 5 of Ref. 4).

In this paper we have also reported absorption results as function of temperature. For standard PPV it is observed that a slight shift as well as a better resolution of the structures on the band occur, when the temperature is lowered from room temperature to 78 K.

This is interpreted (see Fig. 9) by different values of the damping factors γ_n as well as of the parameters of the distribution (see Tables II and III), indicating a slight increase of the length of the conjugated segments and of the weight of G. A decrease in temperature would therefore increase the order in the film, as also suggested elsewhere in literature,[9] with the consequence of decreasing γ_n and increasing the effective conjugation length. This is an important point because, for luminescence data obtained in PPV at different

temperatures [Figs. 2(d) and 2(e)], similar effects are also seen in terms of shift and resolution of the structures of the band. As discussed previously, this can be also interpreted by the use of a distribution of segment lengths, and in particular by the main role played by the longest segments in the distribution in determining the onset of the emission.

A further example is given by the luminescence spectra of standard and ''improved'' PPV shown in Fig. 3 of Ref. 11, in which the onset of the emission is the same, at a given temperature (300 or 77 K). This is an argument in favor of the hypothesis that the relaxed state is the same in both samples, in agreement with the parameter values for the intermediate segment distribution used in the calculations presented in this paper. In fact, Raman and absorption data for the two samples (see Figs. 8, 10, and 11) are interpreted in terms of distributions (Table III) whose sets of parameters are characterized by a very different value of G, but by the same value of the maximum of intermediate length segment distribution. Thus, even if the weight of the intermediate segments is very different in the two cases at a given temperature, the relaxed states must be the same in the two samples at the same temperature.

ACKNOWLEDGMENTS

We would like to thank J. Cornil and his collaborators for using their experimental data. The ''Institut des Matériaux de Nantes'' is Unité Mixte de Recherche No. 6502 CNRS/Université de Nantes.

[1] G. R. Mölhmann, Synth. Met. **67**, 77 (1994).
[2] D. R. Baigent, N. C. Geenham, J. Grüner, R. N. Marks, R. H. Friend, R. C. Moratti, and A. B. Holmes, Synth. Met. **67**, 3 (1994).
[3] J. Bullot, B. Dulieu, and S. Lefrant, Synth. Met. **61**, 211 (1993).
[4] J. Wery, B. Dulieu, J. Bullot, M. Baitroul, Ph. Deniard, and J. P. Buisson, Polymer **40**, 519 (1999).
[5] J. Cornil, D. Beljonne, Z. Schuai, T. W. Hagler, J. Campbell, D. D. C. Bradley, J. L. Brédas, C. W. Spangler, and K. Müller, Chem. Phys. Lett. **247**, 425 (1995).
[6] I. Orion, J. P. Buisson and S. Lefrant, Phys. Rev. B **57**, 7050 (1998).
[7] G. P. Brivio and E. Mulazzi, Phys. Rev. B **30**, 876 (1984).
[8] S. Lefrant, F. Faulques, G. P. Brivio, and E. Mulazzi, Solid State Commun. **53**, 583 (1985).
[9] J. Yu, H. Hayashi, S. H. Lin, K. K. Liang, J. H. Hsu, W. S. Fann, C. L. Chao, K. R. Chuang, and S. A. Chen, Synth. Met. **32**, 159 (1996).
[10] J. Yu, N. S. Farm, F. J. Kao, D. Y. Yang, and S. H. Lin, Synth. Met. **66**, 143 (1994).
[11] K. Pichler, D. A. Halliday, D. D. C. Bradley, P. L. Burn, R. H. Friend, and A. B. Holmes, J. Phys.: Condens. Matter **5**, 7155 (1993).
[12] E. Mulazzi, A. Ripamonti, C. Godon, and S. Lefrant, Phys. Rev. B **57**, 15 328 (1998).